AIRS Deconvolution and the Translation of AIRS to CrIS Radiances with Applications for the IR Climate Record

Howard E. Motteler, *Member, IEEE,* L. Larrabee Strow

***Abstract*—Spectra of the earth's thermal emission as measured by the AIRS, CrIS, and IASI hyper-spectral sounders are becoming a significant part of the long term climate record. These instruments have broadly similar spatial sampling, spectral resolution, and band spans. However the spectral response functions differ in detail, leading to significant differences in observed spectra. To address this we translate channel radiances from one sounder to another, including simulation of the response functions of the translation target. We make regular use of such translations from AIRS to CrIS and IASI to CrIS, and have implemented and tested IASI to AIRS and CrIS to AIRS translations as well. Our translation from AIRS to CrIS has some novel features. AIRS is a grating spectrometer with a distinct response function for each channel, whereas CrIS is a Michaelson interferometer with a sinc response function after calibration and corrections. We use our detailed knowledge of the AIRS spectral response functions to deconvolve AIRS channel radiances to a resolution enhanced intermediate representation. This is reconvolved to CrIS or other instrument specifications. The resulting translation is shown to be more accurate than interpolation or regression.**

***Index Terms*—AIRS, CrIS, deconvolution, hyperspectral, IR sounder, spectral response function.**

I. Introduction

Spectra of the earth's thermal emission as measured by the AIRS [1], CrIS [2], [3], and IASI [4] hyperspectral infrared sounders are becoming a significant part of the long term climate record. Such measurements began with AIRS in 2002 and should continue for the foreseeable future, given their important role in numerical weather prediction. These sounders are in sun-synchronous near-polar orbits, with broadly similar spatial sampling, spectral resolution, and spectral band spans. However the spectral response functions vary in detail, and this can lead to significant differences in observed spectra.

For applications such as calibaration and validation, retrievals, and the construction of a long term climate record we would like to work with single set of spectral response functions. This is can be done by translating channel radiances from one sounder to another, including simulation of the response functions of the translation target. We make regular use of translations from AIRS to CrIS and IASI to CrIS, and have implemented and tested IASI to AIRS and CrIS to AIRS translations as well. The translations from IASI includes deapodization (a form of deconvolution) before reconvolution to the translation target, and work very well. Ranking these translations by accuracy in comparison with calculated reference truth, we have IASI to CrIS, IASI to AIRS, AIRS to CrIS, and finally CrIS to AIRS [5]. But aside from the AIRS to CrIS translation the methods used are for the most part conventional.

Our translation from AIRS to CrIS has some novel features. AIRS is a grating spectrometer with a distinct response function for each channel determined by the focal plane geometery, whereas CrIS is a Michaelson interferometer with a sinc response function after calibration and corrections. In section II we show how to take advantage of our detailed knowledge of the AIRS spectral response functions (SRFs) and their overlap to deconvolve channel radiances to a resolution-enhanced intermediate representation, typically a 0.1 cm^{-1} grid, the approximate resolution of the tabulated AIRS SRFs. This intermediate representation can then be reconvolved to an alternate instrument specification. Section III gives details and validation tests for an AIRS to CrIS translation, and section IV for translation from AIRS to an idealized grating model. Both translations can be further improved with a statistical correction. In section V we consider conventional and principal component regression for an AIRS to CrIS translation, and compare this with our deconvolution-based translation.

II. AIRS Deconvolution

The AIRS spectral response functions model channel response as a function of frequency and associate channels with nominal center frequencies. Each AIRS channel i has an associated spectral response function or SRF $\sigma_i(v)$ such that the channel radiance $c_i = \int \sigma_i(v) r(v)\, dv$, where r is radiance at frequency v. The center or peak of σ_i is the nominal channel frequency.

Figure 1 shows typical AIRS SRFs from the low and high ends of the band. Note the significant overlap in the wings. This allows the deconvolution to recover resolution beyond that of the response functions considered individually. The SRFs are not necessarily symmetrical, especially at the high end of the band, due to fringing from the AIRS entrance filters. The dashed line on top of the third SRF in each group is a fit for a generalized Gaussian [6] of the form

$$w(v, v_0, \text{FWHM}) = \exp\left(-\left(\frac{(v - v_0)^2}{2s^2}\right)^p\right),$$

Submitted 22 March 2018. This work was funded in part by the NASA Earth Sciences Intercalibration Program Grant NNX16AQ68G.

L. Larrabee Strow is Research Professor with the Department of Physics, University of Maryland Baltimore County, Baltimore MD 21250, email strow@umbc.edu.

Howard E. Motteler is Research Asociate Professor with the Joint Center for Earth Systems Technology, 5523 Research Park Drive Suite 140, Baltimore MD 21228, email motteler@gmail.com.

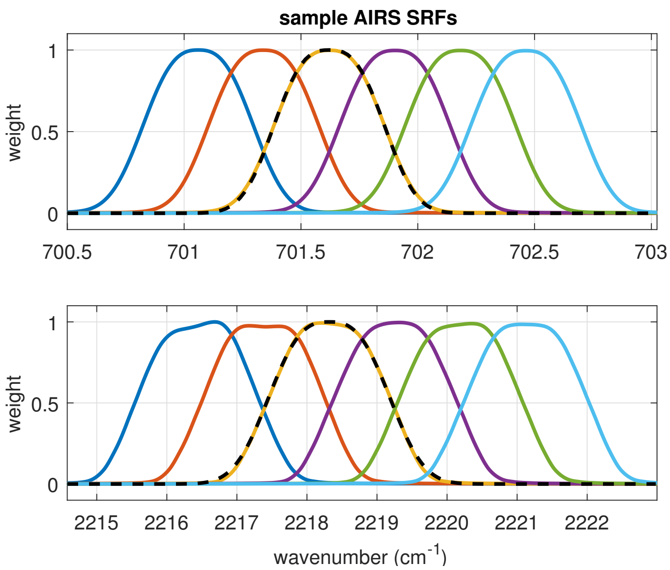

Fig. 1. Sample AIRS spectral response functions from the low and high ends of the band. The dashed line is a generalized Gaussian function.

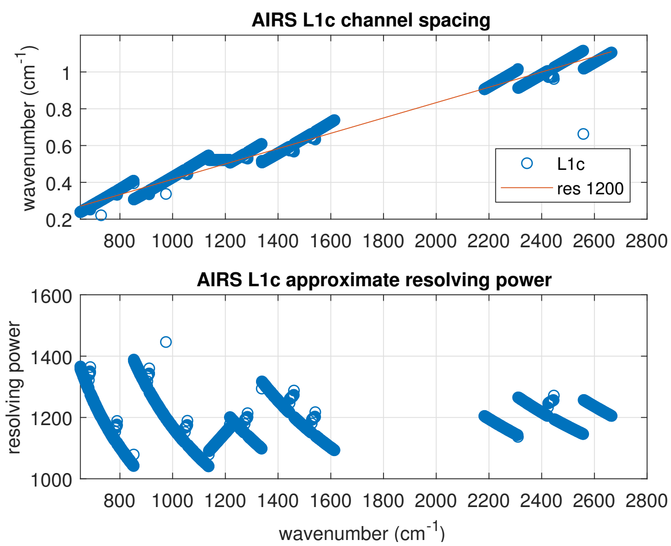

Fig. 2. AIRS L1c channel spacing and resolving power, $R = v_i/\text{FWHM}_i$. The relatively regular L1c channel spacing aids the deconvolution.

where $s = \text{FWHM}/(2\sqrt{2}\,(\ln 2)^{1/(2p)})$. Parameters v, v_0 and FWHM are frequency, desired channel center, and desired full width half max. We chose $p = 1.4$ to give an approximate match to AIRS SRFs, though without the variation or extended tails of the measured SRFs. We will use this analytic representation to calculate reference truth for the deconvolution and in section IV as the basis for an idealized grating model.

Figure 2 shows channel spacing and resolving power for the AIRS L1c channel set [7]. The variable channel spacing and resolving power are due to the modular structure of the focal plane. Although not entirely regular—that is, not a simple function of frequency—the L1c channel set is more regular than the L1b channel set from which it is derived, and we mainly consider the L1c set here.

Suppose we have n channels and a frequency grid $\vec{v}$ of k points spanning the union of the domains of the functions σ_i. The grid step size for our applications is often 0.0025 cm^{-1}, the default resolution for upwelling radiances calculated using the kCompressed Atmospheric Radiative Transfer Model (kCARTA) [8]. Let S_k be an $n \times k$ array such that $s_{i,j} = \sigma_i(v_j)/w_i$, where $w_i = \sum_j \sigma_i(v_j)$, that is where row i is $\sigma_i(v)$ tabulated at the grid $\vec{v}$ and normalized so the row sum is 1. If the channel centers are in increasing order S_k is banded, and if they are not too close (as is the case for a few of the L1b channels) the rows are linearly independent. S_k is a linear transform whose domain is radiance at the grid $\vec{v}$ and whose range is channel radiances. If r is radiance at the grid $\vec{v}$, then $c = S_k r$ gives a good approximation of the channel radiances $c_i = \int \sigma_i(v) r(v)\, dv$. In practice this is how we calculate AIRS channel radiances for the validation tests described in subsequent sections.

For the AIRS to CrIS and other translations we are mainly interested in the transform S_b for SRFs at an intermediate resolution, typically $0.1\ \text{cm}^{-1}$. This is the approximate resolution of the SRF measurements and convenient for reconvolution to the CrIS user grid. So let $\vec{v}_b = v_1, v_2, \ldots, v_m$ be a $0.1\ \text{cm}^{-1}$ grid spanning the domains of the functions σ_i. Similar to S_k, let S_b be an $n \times m$ array where row i is $\sigma_i(v)$ tabulated at the $\vec{v}_b$ grid, with rows normalized to 1. If r is radiance at the $\vec{v}_b$ grid, then $c = S_b r$ is still a reasonable approximation of $\int \sigma_i(v) r(v)\, dv$.

For our application we want to start with c and find r, that is to deconvolve c by solving $S_b r = c$ for r. Since $n < m$, the system is underdetermined. We take the Moore-Penrose pseudoinverse [9], [10] of S_b to get $r_0 = S_b^{-1} c$. This gives a minimal solution, in the sense that $||r_0||_2 \leq ||r_j||_2$ for all r_j satisfying $S_b r_j = c$. The condition number for S_b as built from the L1c channels is $||S_b||_2 ||S_b^{-1}||_2 = 115$, which is tolerable.[1]

Although our main goal is to reconvolve the deconvolved AIRS radiances to the CrIS or other user grids, as a check we first compare the deconvolved radiances with reference truth from a direct convolution of kCARTA radiance to the $0.1\ \text{cm}^{-1}$ grid. The response function we use for this is the generalized Gaussian above with $\text{FWHM} = v_i/2000$, where v_i are the grid frequencies. This represents a hypothetical grating spectrometer with a resolving power of 2000, oversampled to the $0.1\ \text{cm}^{-1}$ grid.

The AIRS deconvolution gives a modest resolution enhancement, at the cost of added artifacts and noise. Figure 3 shows spectra from fitting profile 1 [12], [13] for the AIRS deconvolution together with reference truth, with sample details from the low and high ends of the band. The ringing or overshoot at 2310 cm^{-1} is due to a change in the L1c channel spacing from 1.02 cm^{-1} to 0.92 cm^{-1} at that point. Figure 4 shows details of kCARTA, the reference convolution, deconvolution, and AIRS spectra for fitting profile 1. In the first subplot we see the deconvolution is capturing some of the fine structure in the kCARTA data that is present in the reference convolution but not the AIRS data. In the second subplot we see the deconvolution (and reference convolution)

[1]The notation $||S||_2$ is the L^2 norm of S, and is simply Euclidian distance for vectors. [11].

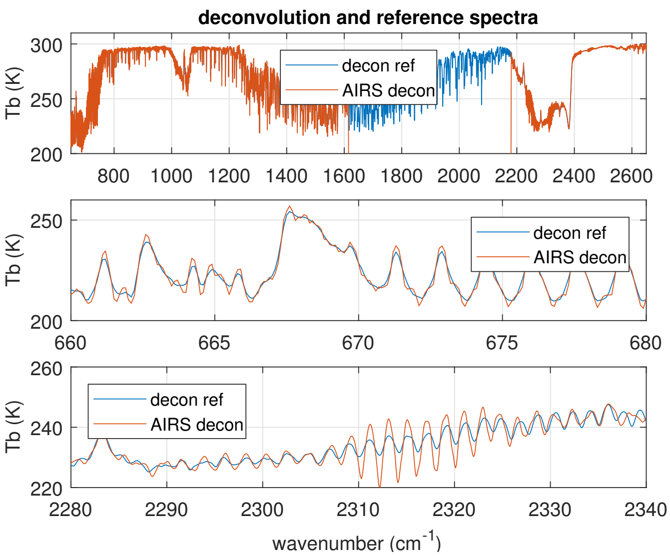

Fig. 3. Spectra from fitting profile 1 for deconvolved AIRS and the reference convolution to the 0.1 cm^{-1} grid. We see some overshoot and ringing in the deconvolution.

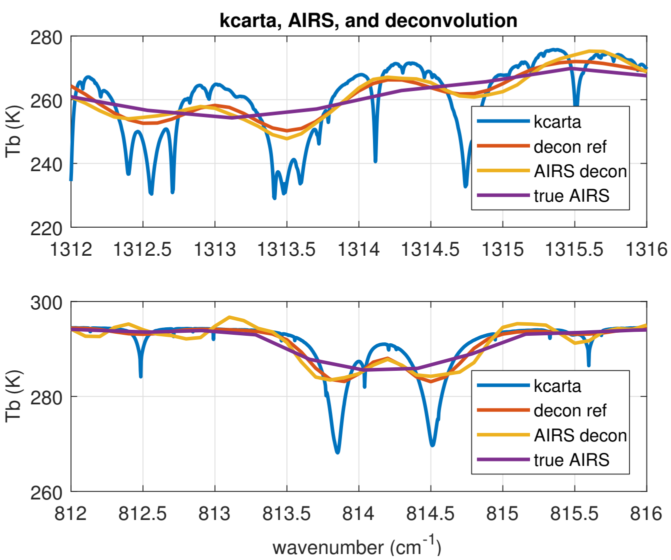

Fig. 4. Details from fitting profile 1 for kCARTA, the reference convolution to the 0.1 cm^{-1} grid, deconvolved AIRS, and true AIRS. The deconvolution restores some detail.

resolving a pair of close lines that are not resolved at the AIRS L1c resolution. But we also see some ringing that is not present in the reference convolution. This is to be expected; significant detail is lost in the convolution to AIRS channel radiances and this can only partially be recovered by the deconvolution. The artifacts are acceptable because we do not propose using the deconvolved radiances directly; they are an intermediate step before reconvolution to a lower resolution.

Figure 5 shows a pair of typical adjacent rows of the deconvolution matrix S_b^{-1} in the first subplot. Row i of S_b^{-1} is the weights applied to L1c channel radiances to synthesize the deconvolved radiance r_i at the intermediate grid frequency v_i. The oscillation shows we are taking the closest AIRS channel, subtracting weighted values for channels ± 1 step

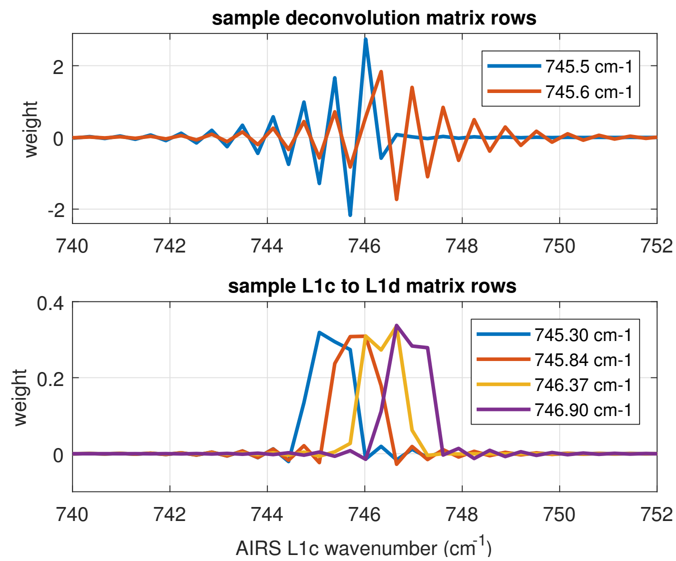

Fig. 5. Sample adjacent rows for the deconvolution and L1c to L1d transforms

away, adding weighted values for channels ± 2 steps away, and so on, with the weights decreasing quickly as we move away from v_i, with eight to ten L1c channels making a significant contribution to each deconvolution grid point. The second subplot shows four adjacent rows of the matrix $S_d \cdot S_b^{-1}$, which takes L1c to L1d channel radiances. (The L1d radiances are discussed in a later section; here they are of interest mainly as a typical reconvolution.) Both matrices are banded but the bands are narrower in the second, with three to five L1c channels contributing to each L1d channel. This span of influence gives us the set of parents for each translated channel.

III. AIRS to CrIS translation

Given AIRS deconvolution to a 0.1 cm^{-1} intermediate grid, reconvolution to the CrIS user grid is straightforward. For CrIS standard resolution the channel spacing is 0.625 cm^{-1} for the LW band, 1.25 cm^{-1} for the MW, and 2.5 cm^{-1} for the SW. For each CrIS band, we (1) find the AIRS and CrIS band intersection, (2) apply a bandpass filter to the deconvolved AIRS radiances restricting them to the intersection, with a rolloff outside the passband, and (3) reconvolve the filtered spectra to the CrIS user grid with a zero-filled double Fourier transform [14]. The out-of-band rolloff smooths what would otherwise be an impulse at the band edges, reducing ringing in the translation.

Translations are tested by comparison with calculated reference truth. We start with a set of atmospheric profiles and calculate upwelling radiance at a 0.0025 cm^{-1} grid with kCARTA [8] over a band spanning the domains of the AIRS and CrIS response functions. "True AIRS" is calculated by convolving the kCARTA radiances with AIRS SRFs and "true CrIS" by convolving kCARTA radiances to a sinc basis at the CrIS user grid. True AIRS is then translated to CrIS to get "AIRS CrIS", and this is compared with true CrIS. Figure 6 shows sample spectra for true AIRS, deconvolved AIRS, true CrIS and AIRS CrIS. Any difference between true CrIS and

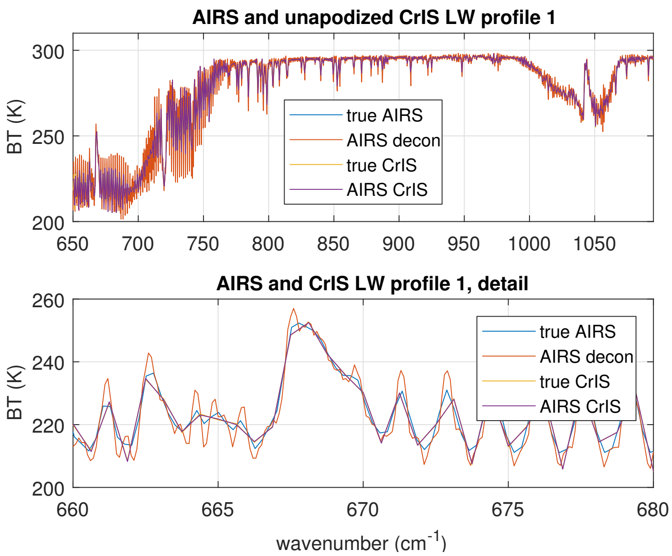

Fig. 6. True AIRS, deconvolved AIRS, true CrIS, and AIRS CrIS. Differences between true CrIS and AIRS CrIS are too small to be visible in this figure.

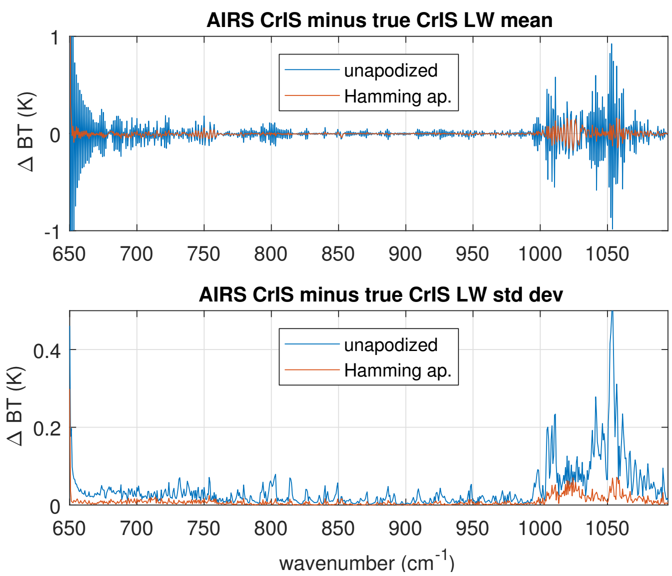

Fig. 7. Mean and standard deviation of unapodized and Hamming apodized AIRS CrIS minus true CrIS, for the LW band.

AIRS CrIS is hard to see here, and in subsequent plots we mainly show explicit differences.

Comparisons are done both with and without apodization. Hamming apodization [15], [16] sacrifices some resolving power but gives a significant reduction in the residuals and is convenient for many applications. Convolution, deconvolution, and apodization are done with radiances, while spectra are presented and statistics are done after conversion to brightness temperatures.

We use radiance from a set of 49 fitting profiles spanning a wide range of clear atmospheric conditions as our test set, and as the independent set for statistical sets. This set was initially chosen for testing radiative transfer codes [12], [13] and is highly uncorrelated; reducing the reconstruction residual to 0.02 K requires 48 left-singular vectors. (Details of this

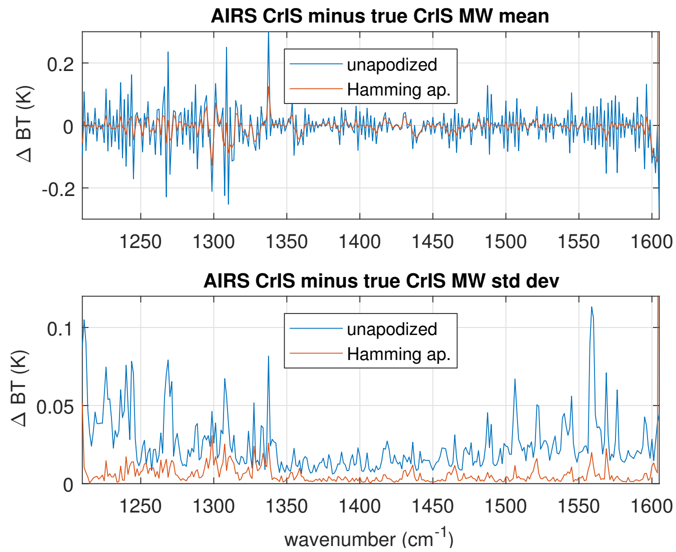

Fig. 8. Mean and standard deviation of unapodized and Hamming apodized AIRS CrIS minus true CrIS, for the MW band.

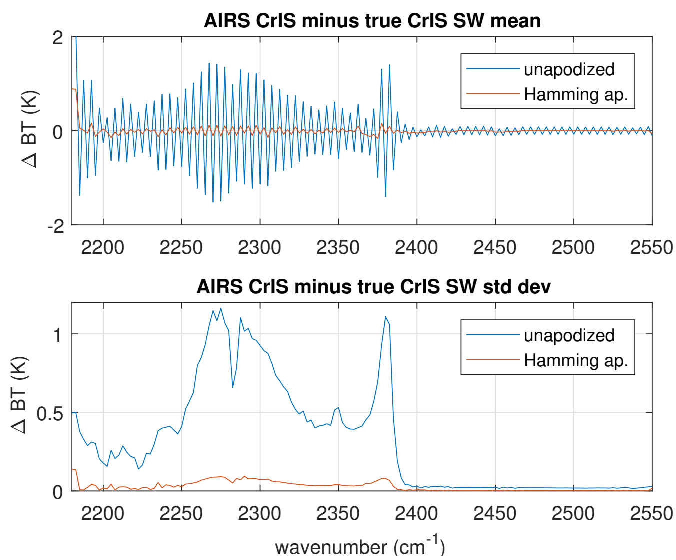

Fig. 9. Mean and standard deviation of unapodized and Hamming apodized AIRS CrIS minus true CrIS, for the SW band.

correlation measure are given in an appendix.) For regression tests we use radiance from a set of 7377 all-sky (clear and cloudy) AIRS profiles spanning several consecutive days as our dependent set. This set is more correlated; reducing the reconstruction residual to 0.02 K requires 260 left-singular vectors. We did try splitting the 7377 profile set into dependent and independent subsets. Residuals from this larger independent set were consistently smaller than from the 49-profile set, suggesting the latter makes for a stricter test.

Figures 7, 8, and 9 show the mean and standard deviation of true CrIS minus AIRS CrIS for the 49 fitting profiles, for each CrIS band. The Hamming apodization gives a significant reduction in the residuals. Figure 10 summarizes results all three bands, for apodized radiances. The constant or DC bias is very close to zero for the apodized residuals. Both the apodized and unapodized residuals are significantly less than

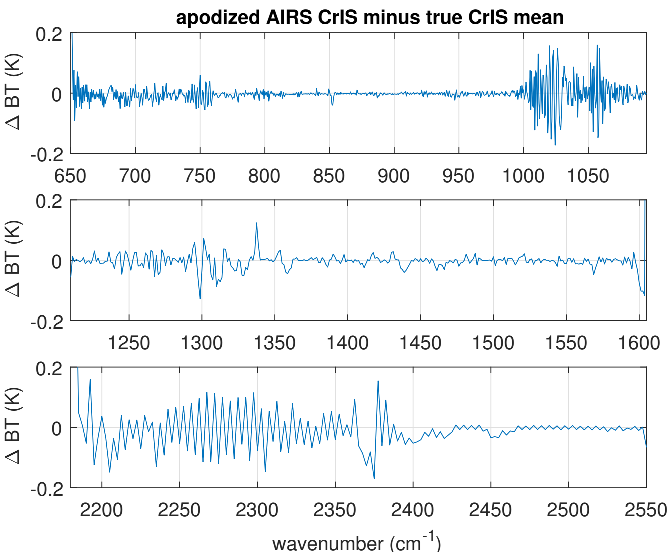

Fig. 10. Summary plot of the mean of apodized residuals for all three CrIS bands, showing the residuals in greater detail.

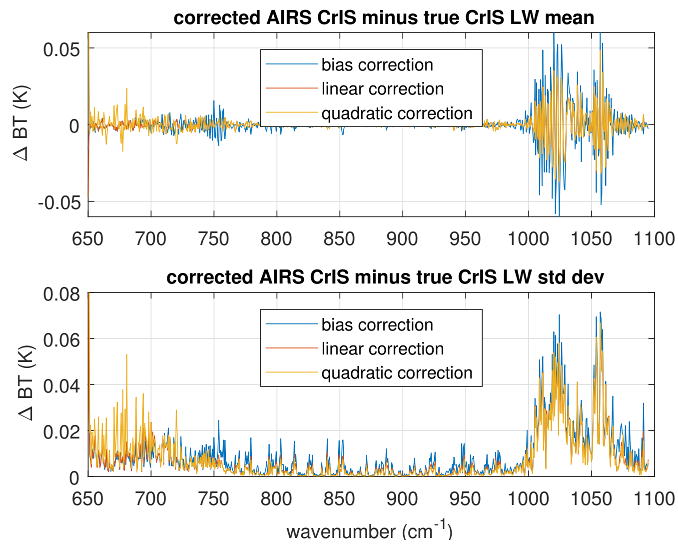

Fig. 11. Mean and standard deviation of corrected apodized AIRS CrIS minus true CrIS, for the LW band.

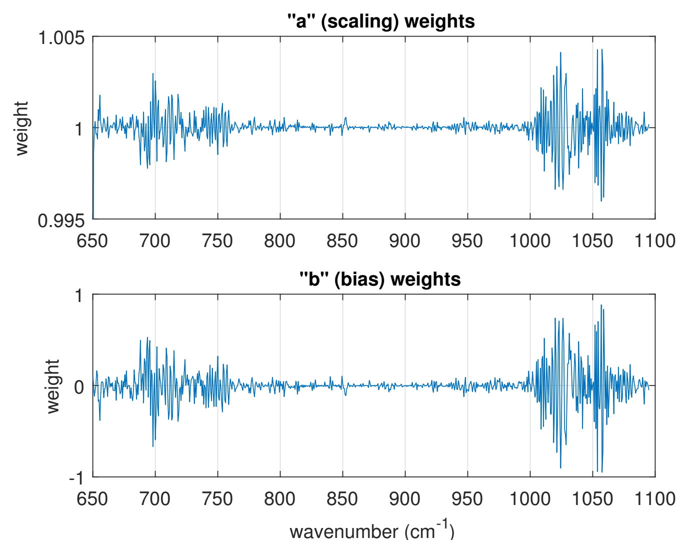

Fig. 12. Weights for the linear correction $ax + b$, for the LW band.

the corresponding residuals from conventional interpolation, as shown in the appendix.

The relatively small standard deviation of the residuals suggests some regularity, and we can see an oscillation with a period of two channel steps in several places. Up to this point there has been no statistical component to our translation, beyond the choice of test set for validation. We feel it is important to be clear about any steps that require statistical fitting. That said, we can use a simple linear correction for a significant further reduction of the residuals. We use the set of 7377 mostly cloudy AIRS profiles as the dependent set and the 49 profile set as the independent or test set.

We compare three such corrections. These are done with a separate regression for each CrIS channel, and so introduce no cross-correlations. Let t_i^{TC} be true CrIS and t_i^{AC} AIRS CrIS brightness temperatures for CrIS channel i, from the dependent set. For the bias test we subtract the mean residual from the dependent set. For the linear test we find a_i and b_i to minimize $||a_i\, t_i^{\text{AC}} + b_i - t_i^{\text{TC}}||_2$, and for the quadratic test weights c_i, a_i and b_i to minimize $||c_i\, (t_i^{\text{AC}})^2 + a_i\, t_i^{\text{AC}} + b_i - t_i^{\text{TC}}||_2$. The resulting correction is then applied to the independent set, the 49 fitting profiles, for comparison with true CrIS.

Figure 11 is a comparison of bias, linear, and quadratic corrections for the LW band. The linear and quadratic corrections are nearly identical, with the quadratic coefficient very close to zero. Figure 12 shows the weights for the linear fits from figure 11. The a weights are very close to 1 and the b weight to the bias. Figures 13 and 14 show the linear correction giving a similar improvement in the MW and a small improvement in the SW, where the quadratic correction is noticably worse. Figure 15 shows the residuals for the apodized linear correction for all three bands. The residuals are significantly reduced in comparison with the apodized uncorrected radiances shown in figure 10 and are generally less than NEdT (for the first fitting profile), as we show next.

We can give a good estimate of noise equivalent differential radiance (NEdN) for the translation by adding noise with a normal distribution at the AIRS NEdN to blackbody radiance at 280K and translating this to CrIS. Figure 16 shows the measured AIRS-to-CrIS NEdN together with AIRS and CrIS NEdN for both apodized and unapodized radiances. The AIRS and CrIS values are averages over a full day, 4 Dec 2016. NEdN for the L1c synthetic channels is interpolated. The first subplot of figure 17 is NEdT for apodized radiances, for fitting profile 1.

Such modeling with normally distributed noise does not take into account correlation in the AIRS noise. The sources of such noise might be vibration, radiation, or any common-mode effect. Details concerning correlation sources are beyond the scope of this paper, except to note that noise for L1c channels with more than one L1b parent may not be well-defined. In practice this is a relatively small set that we may want to use with caution.

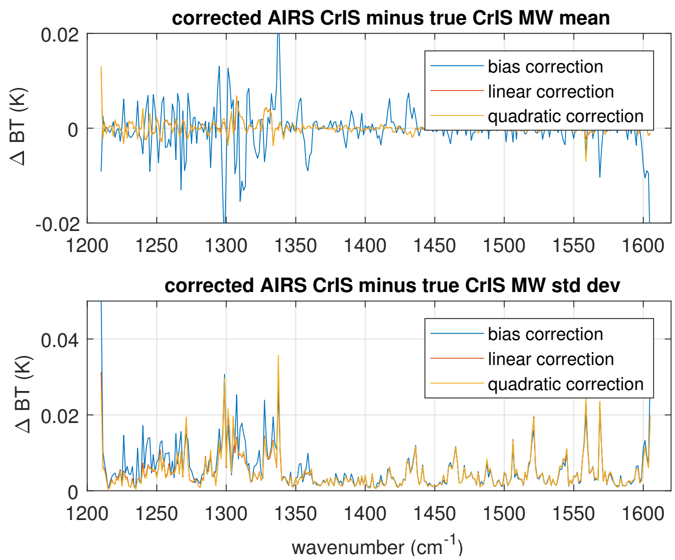

Fig. 13. Mean and standard deviation of corrected apodized AIRS CrIS minus true CrIS, for the MW band.

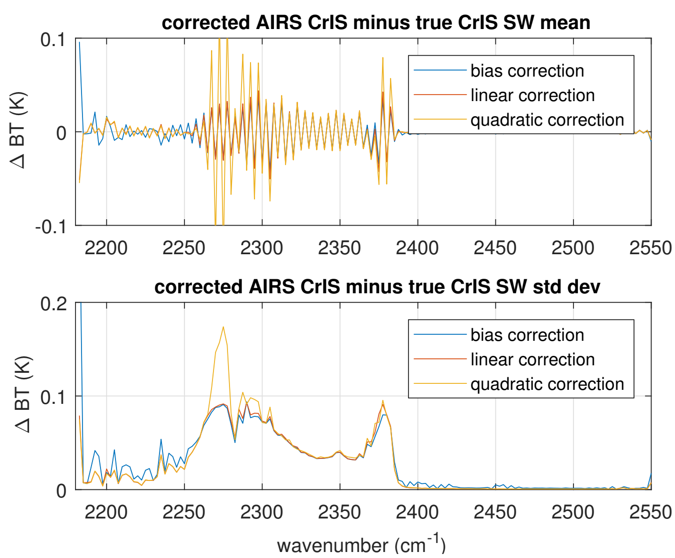

Fig. 14. Mean and standard deviation of corrected apodized AIRS CrIS minus true CrIS, for the SW band.

The AIRS channel-to-channel NEdN variation is significant; in the upper half of the LW and most of the MW it is of the same order as the AIRS and CrIS NEdN difference. This variation is due the AIRS focal plane structure and sensitivity. The AIRS and CrIS NEdN measures are both spiky when averaged over a few minutes but the CrIS variation is primarily uncertainty in the noise measurement and smooths out as the time span is extended, while the AIRS variation is stable. The AIRS-to-CrIS translation inherits this variability; it is a significant part of the difference between AIRS CrIS and true CrIS. For a common record we might want to add noise on a channel-by-channel basis to whichever NEdN value—AIRS CrIS or true CrIS—is lower. NEdN for the combined record would then be max of the AIRS CrIS and true CrIS NEdN values, as shown in the second subplot of figure 17. In the same spirit we could add AIRS correlation, to the extent that

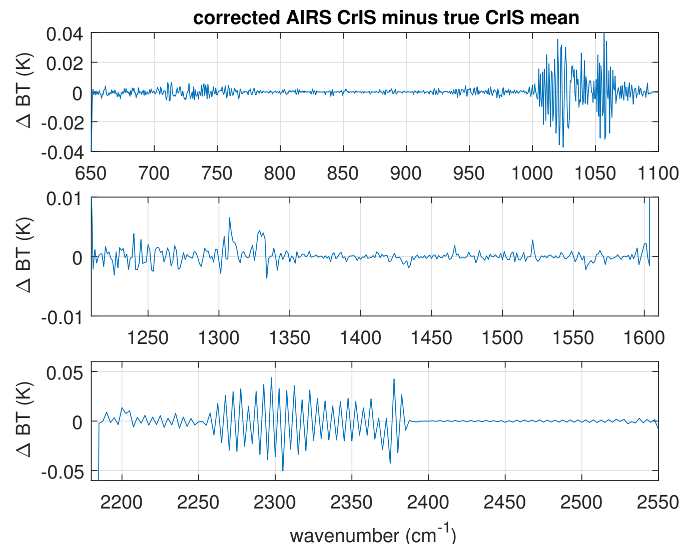

Fig. 15. Mean corrected apodized residuals for all three bands, showing the linear corrected apodized residuals in greater detail.

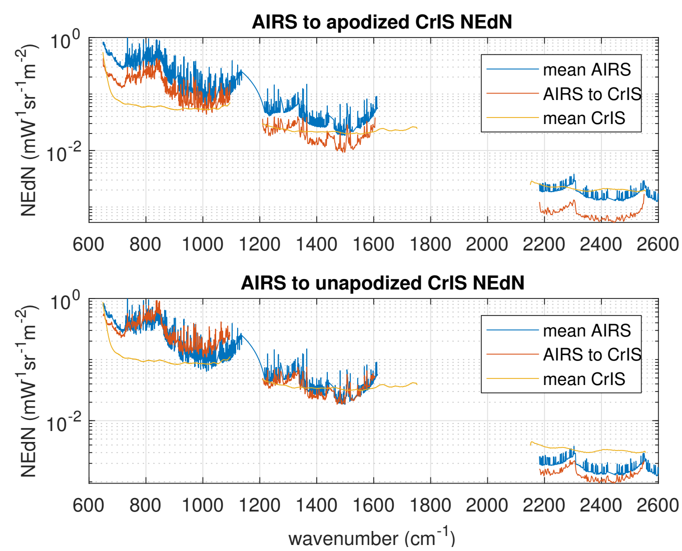

Fig. 16. AIRS, AIRS-to-CrIS, and CrIS NEdN. Apodization reduces the CrIS and AIRS-to-CrIS NEdN by a factor of 0.63.

this is well-defined.

In addition to the standard resolution described above, in December 2014 CrIS switched to a high resolution mode with a nominal OPD of 0.8 cm for all three bands, while continuing to support the standard resolution product. AIRS does not have the resolving power to properly support a translation for the CrIS high resolution MW and SW bands, and the residuals for that translation are relatively large. For a long-term common record one solution might be a compromise CrIS resolution of 0.6 cm for the MW and 0.4 cm for the SW, to roughly match the AIRS resolving power.

As an alternative, in the next section we consider translation from AIRS to an idealized grating model. This requires a translation from both AIRS and CrIS, but so would the compromise CrIS resolutions. The CrIS high resolution mode allows for a CrIS to AIRS translation, as described in [5]. The residuals are

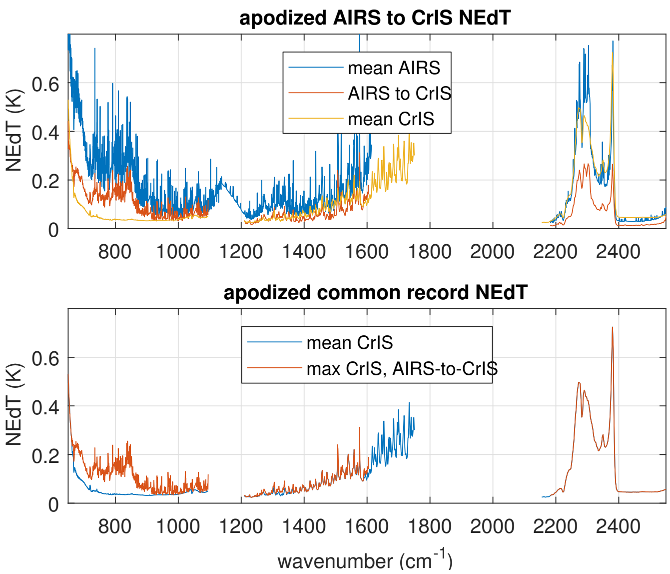

Fig. 17. AIRS, AIRS-to-CrIS, and CrIS apodized NEdT, and the max of CrIS and AIRS-to-CrIS NEdN (shown as NEdT) with CrIS NEdT shown as a reference.

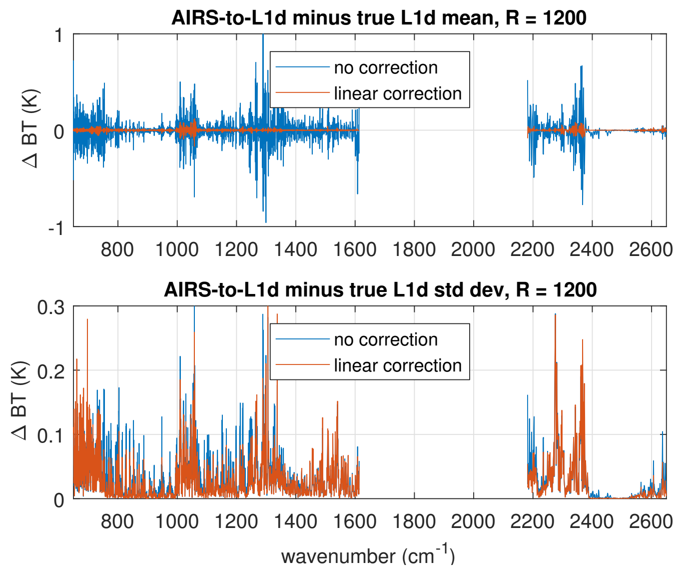

Fig. 18. Mean and standard deviation for the AIRS L1c to L1d translation minus true L1d, for a resolving power of 1200.

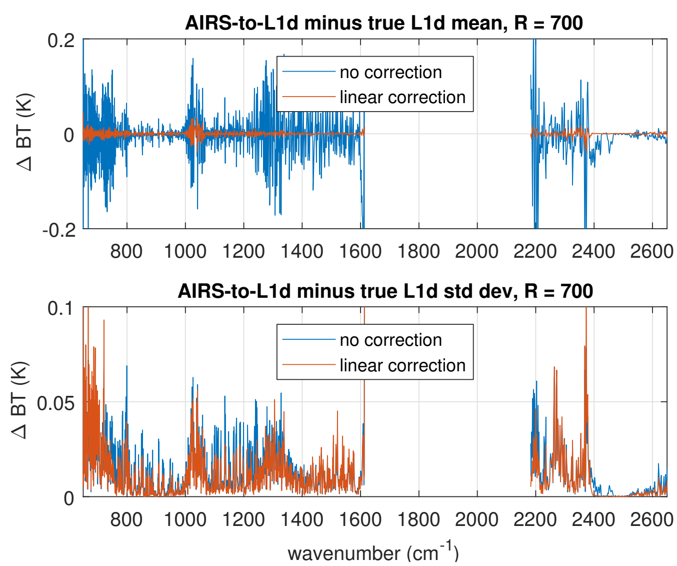

Fig. 19. Mean and standard deviation for the AIRS L1c to L1d translation minus true L1d, for a resolving power of 700.

larger in the LW than for our translation from AIRS to CrIS, but may be acceptable for some applications. A CrIS translation to the proposed idealized grating model should work at least as well.

IV. Translation to an Idealized Grating Model

The AIRS deconvolution can be used for other translations. In this section we briefly examine reconvolution to an idealized grating model for resolving powers of 700 and 1200. There are several reasons to consider such a translation. The constant resolving power of the L1d basis (defined below) makes it a more natural translation target for AIRS than the constant channel spacing of CrIS. It could be considered as the next step in regularization of the AIRS product, following the partial regularization from L1b to L1c, and as a potential alternative target for a long-term common record.

Define an AIRS L1d basis with resolving power R using the generalized Gaussian response function of section II as follows. Let v_0 be the frequency of the first channel, and for $i \geq 0$, $\text{FWHM}_i = v_i/R$, $dv_i = \text{FWHM}_i/2$, and $v_{i+1} = v_i + dv_i$. As with tests of the AIRS to CrIS translation, true L1c is calculated by convolving kCARTA radiances with AIRS L1c SRFs and true L1d by convolving with an L1d basis at the desired resolving power. L1c is translated to L1d by deconvolution followed by reconvolution to the desired L1d basis, and this is compared with true L1d.

Figure 18 shows residuals for reconvolution to an L1d basis with resolving power of 1200, the nominal AIRS resolution, and figure 19 shows residuals for a resolving power of 700. Note the different x-axes for the two figures. The residuals depend in part on the L1d starting channel v_0, and so on how the L1c and L1d SRF peaks line up. The residuals shown are the result of a rough fit for v_0. For a resolving power of 1200 this gave v_0 equal to the first L1c channel, while for 700 it was the first L1c channel plus 0.2 cm^{-1}.

We see that for both the AIRS to CrIS and L1c to L1d translations some resolving power is sacrificed in shifting channel centers to a single regular function of frequency. Residuals for a resolving power of 1200 (figure 18) are roughly comparable to unapodized CrIS (figures 7, 8, and 9) and residuals for a resolving power of 700 (figure 19) are roughly comparable to apodized CrIS (figure 15). As with the AIRS to CrIS translation, the L1c to L1d residuals are significantly reduced with a linear correction. Residuals for L1d with a resolving power of 700 after correction are comparable to residuals for apodized CrIS after a similar correction.

V. Direct and Principal Component Regression

We want to compare our deconvolution-based translations with other approaches to radiance translation, with an empha-

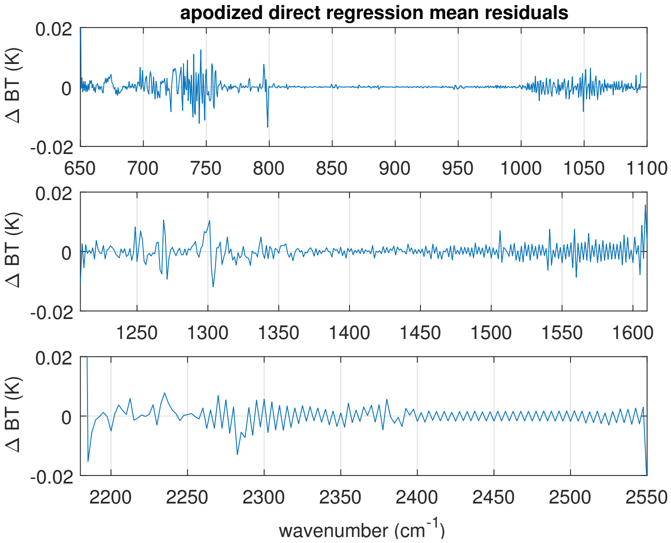

Fig. 20. Mean residuals over the 49 profile independent set for AIRS to apodized CrIS direct regression.

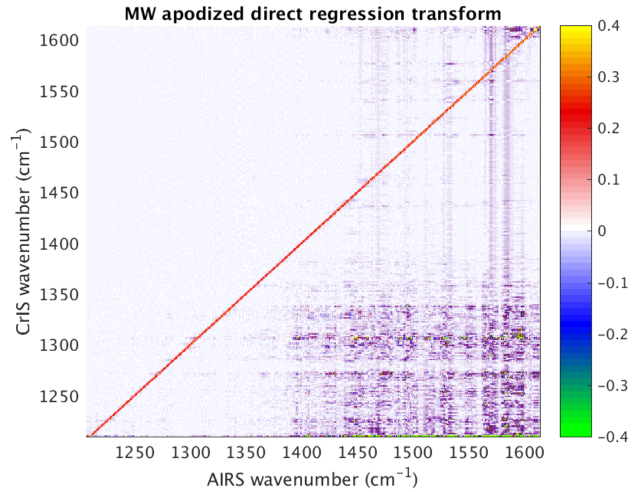

Fig. 21. Regression transform from the 7377 profile dependent set for the MW apodized direct regression transform.

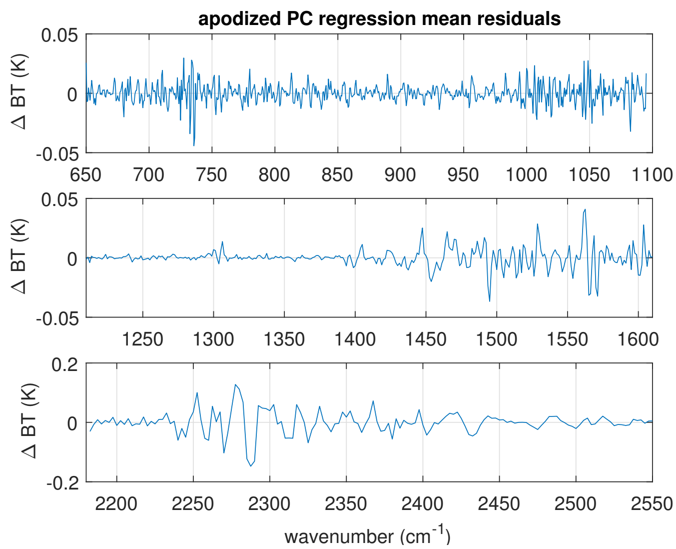

Fig. 22. Mean residuals over the 49 profile independent set for AIRS to apodized CrIS principal component regression.

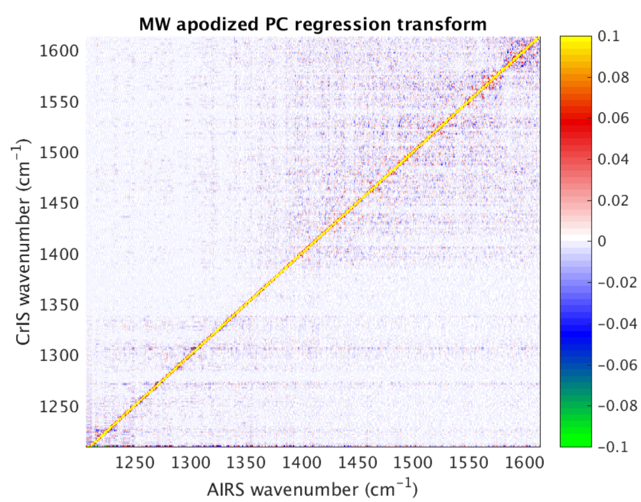

Fig. 23. Regression transform from the 7377 profile dependent set for MW apodized principal component regression with $i = 500$ and $j = 320$.

sis on methods we have used in the past. In this section we consider regression-based translations, and in section VII-B conventional interpolation.

The AIRS L1c to L1d translation can be done with a single linear transform $S_d \cdot S_c^{-1}$, where S_c and S_d are the transforms taking the intermediate grid to L1c and L1d channels. The AIRS to CrIS translation could also be done with a composite transform if we use a resampling matrix rather than double Fourier interpolation and a matrix form of the bandpass filters. We can get such a one-step tranform in other ways. Suppose r_a and r_c are $m \times k$ and $n \times k$ AIRS and CrIS radiance sets, for example true AIRS and true CrIS from section III. We can find an $n \times m$ matrix X by regression to minimize $\|X r_a - r_c\|_2$ and use this as our AIRS to CrIS transform. We call this standard technique "direct regression" here. This is different from the corrections of section III and IV; there regression was used to find linear or quadratic correction coefficients independently for each channel.

Figures 20 shows residuals for direct regression from AIRS to apodized CrIS radiances. As before we use the 7377 profile set as the dependent set and the 49 profile set as the independent set. The residuals are roughly comparable to the residuals from the deconvolution translation summarized in figure 15. However the regression matrices show significant off-diagonal correlations. Figure 21 shows this for the MW band; correlations are less for the LW and larger for the SW. In addition, the dependent set residuals are very small, much less than the residuals for the independent set. These are signs of over-fitting. As noted in section III the 7377 profile dependent set is highly correlated; the effective dimension (as defined in the appendix) is only 260.

Common techniques for reducing such correlation include adding noise, restricting the solution to a banded matrix, or working with principal component decompositions of the data. We had best results with the latter. As above let r_a and r_c be $m \times k$ and $n \times k$ AIRS and CrIS radiance sets. Let $r_a = U_a S_a V_a^T$ be the singular value decomposition with singular values in descending order and U_a^i the first i columns of U_a. Similarly let $r_c = U_c S_c V_c^T$ be a singular value decomposition with singular values in descending order and U_c^j the first j columns of U_c. Let $\hat{r}_a = (U_a^i)^T r_a$ and $\hat{r}_c = (U_c^j)^T r_c$ be r_a and r_c represented with respect to the bases U_a^i and U_c^j. (Since the bases are orthonormal, the transpose is the inverse.) Then as before find X by regression to minimize $\|X\hat{r}_a - \hat{r}_c\|_2$. This gives us $R = U_c^j X (U_a^i)^T$, an AIRS to CrIS transform parameterized by the basis sizes i and j.

Note that our principal component regression is not the same as regression after principal component (or singular vector) filtering; for that we would take $\bar{r}_a = U_a^i (U_a^i)^T r_a$, $\bar{r}_c = U_c^j (U_c^j)^T r_c$, find X to minimize $\|X\bar{r}_a - \bar{r}_c\|_2$, and have no need for a change of bases to apply X. In practice this did not work as well as doing regression after the change of bases.

Figure 22 shows residuals and figure 23 the transform R for the CrIS MW band. We have chosen $i = j = 500$ for the LW, $i = 500$ and $j = 320$ for the MW, and $i = j = 100$ for the SW for the basis sizes, to roughly balance unwanted correlation with residual size. The off-diagonal correlations are significantly reduced, but the residuals are now larger than for the deconvolution-based translation summarized in figure 15. We conclude that principal component regression works fairly well, in comparison with regular regression or interpolation, but not quite as well as the deconvolution-based translation.

VI. Applications

We have been using the AIRS to CrIS and IASI to CrIS translations to analyze simultaneous nadir overpasses (SNOs) [17], [18] and hope to create a long-term climate record spanning observations from multiple sounders. The translation of response functions as discussed here is just one part of such a project. To build a common record we must choose a target format. This might be CrIS standard resolution, a CrIS intermediate resolution as proposed in section III, or the generalized Gaussian basis of section IV. The choice constrains which sounders or resolution modes can be included. For example, our proposed CrIS 0.8/0.6/0.4 cm^{-1} intermediate resolution would mean dropping two and a half years (April 2012 to November 2014) of overlap of AIRS and CrIS standard resolution data. This sort of problem is inherent in building a common record—over time resolving power and band spans typically increase. But a target format is constrained by what is available from the start.

Uniform spatial sampling is a key part of a long-term record. AIRS and CrIS sampling is similar but not identical. Details are beyond the scope of this paper, but some subsetting is typically necessary. For example most of our sampling analysis is downstream from a “latitude weighted subset”, the selection of all observations such that $X < |\cos(\text{latitude})|$, where X is a random variable from the uniform distribution $[0, 1]$ [19]. Further subsetting, to correct for sampling biases or simply to save space, may be desirable.

For some applications these translations allow the use of a common radiative transfer model and retrieval algorithm. For applications such as assimilation and physical retrievals the translation would need added noise, as discussed in section III. Finally, a possible future application is to revisit the AIRS SRF measurements, to see if adjustments (within the original measurement uncertainty) can reduce the translation residuals.

VII. Appendix

A. Measures of correlation

We want to measure the correlation of a set of radiances. One such measure is dimension of a spanning set. For an approximation we use the basis size needed to get reconstruction residuals below some fixed threshold. Let r_0 be an $m \times n$ array of radiances, one row per channel and one column per observation. Let $r_1 = USV^T$ be a singular value decomposition with singular values in descending order and U_k the first k columns of U. Let $r_k = U_k U_k^T r_0$; then $r_k \approx r_0$. The approximation improves as k increases and becomes exact for some $k <= m$. This is the analog of principal component filtering using left-singular rather than eigenvectors and is useful as a form of compression when k is small relative to n. For that case we save U_k and $U_k^T r_0$ separately. Applications include compression of IASI radiance data and the kCARTA absorption coefficient database.

We use a threshold for equivalence that is relevant for our applications. Let B^{-1} be the inverse Planck function and define $d(r_1, r_2) = \text{RMS}(B^{-1}(r_1, v) - B^{-1}(r_2, v))$, the RMS difference over all channels and observations of the brightness temperatures of radiance data. Finally let j be the smallest value such that $d(r_0, r_j) \leq T_d$, for some threshold T_d. Then j is the effective dimension of our set r_0. Here we have chosen $T_d = 0.02$ K. For the 49 profile fitting set this gives $j = 48$, which we interpret as largely uncorrelated, while for the 7377 profile cloudy set we found $j = 260$, which we interpret as highly correlated.

B. Conventional interpolation

The AIRS to CrIS translation via deconvolution works significantly better than conventional interpolation. This is not surprising since the former makes use of both the source and target response functions. We consider two cases. For the first, start with true AIRS and interpolate radiances directly to the CrIS user grid with a cubic spline. This makes no use of either the AIRS or CrIS response functions. For the second, interpolate true AIRS to the 0.1 cm^{-1} intermediate grid with a cubic spline and then convolve this to the CrIS user grid. This uses the CrIS but not the AIRS response functions. Results for apodized CrIS LW radiance are summarized in Figure 24. As expected, residuals for spline interpolation alone are larger that for spline interpolation followed by convolution to the CrIS user grid, and both are significantly larger than residuals for AIRS deconvolution followed by the CrIS convolution. Results for the MW and SW are similar.

The AIRS L1c to L1d translation via deconvolution also works significantly better than interpolation. As before, we consider two cases. For the first, start with true AIRS and interpolate radiances directly to the L1d grid with a cubic spline. For the second, interpolate true AIRS to the 0.1 cm^{-1} intermediate grid with a cubic spline and convolve this to the

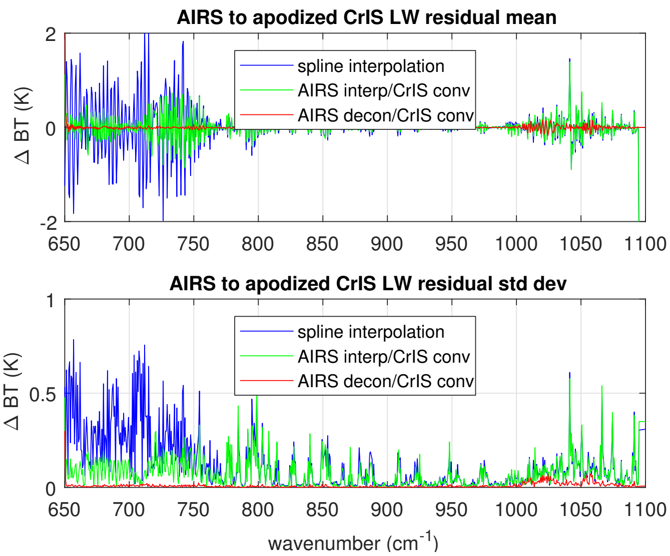

Fig. 24. The AIRS to apodized CrIS translation via spline interpolation, interpolation followed by CrIS convolution, and AIRS deconvolution followed by CrIS convolution.

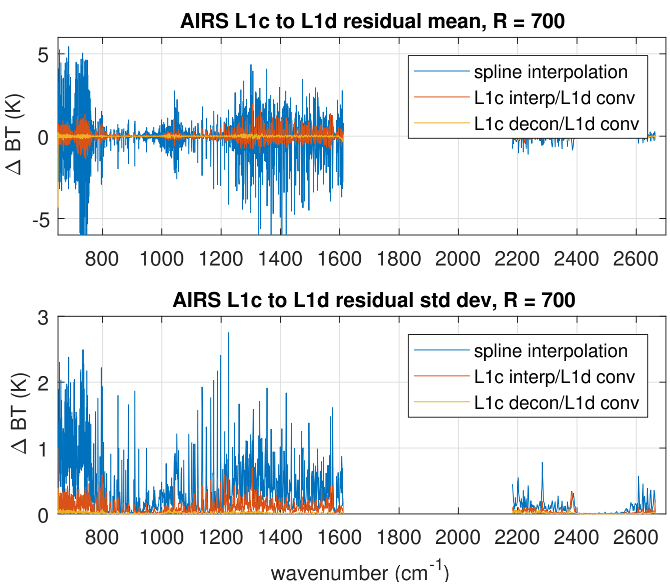

Fig. 25. The AIRS L1c to L1d translation via spline interpolation, interpolation followed by CrIS convolution, and AIRS deconvolution followed by CrIS convolution.

L1d channel set. Results for a resolving power of 700 are summarized in Figure 25. Residuals for spline interpolation are larger that for spline interpolation followed by convolution to the L1d channel set, and both are significantly larger than residuals for AIRS deconvolution followed by the L1d convolution.

C. Source code

Matlab code for the translations and tests described here (including the IASI to CrIS, IASI to AIRS, and CrIS to AIRS translations mentioned in the introduction) is available at GitHub:

- https://github.com/strow/airs_deconv
- https://github.com/strow/iasi_decon

The translations have been tested extensively. Runtime for the AIRS to CrIS translation is split fairly evenly between deconvolution and reconvolution. It takes about 30 seconds to translate our 7377 profile cloudy set running on one processor. Calculating the pseudo-inverse adds another 10 seconds, but that only needs to be done when the translation parameters change.

REFERENCES

[1] H. H. Aumann, M. T. Chahine, C. Gautier, M. D. Goldberg, E. Kalnay, L. M. McMillin, H. Revercomb, P. W. Rosenkranz, W. L. Smith, D. H. Staelin, L. L. Strow, and J. Susskind, "AIRS/AMSU/HSB on the aqua mission: design, science objectives, data products, and processing systems," *IEEE Transactions on Geoscience and Remote Sensing*, vol. 41, pp. 253–264, Feb. 2003.

[2] Y. Han, H. Revercomb, M. Cromp, D. Gu, D. Johnson, D. Mooney, D. Scott, L. Strow, G. Bingham, L. Borg, Y. Chen, D. DeSlover, M. Esplin, D. Hagan, X. Jin, R. Knuteson, H. Motteler, J. Predina, L. Suwinski, J. Taylor, D. Tobin, D. Tremblay, C. Wang, L. Wang, L. Wang, and V. Zavyalov, "Suomi NPP CrIS measurements, sensor data record algorithm, calibration and validation activities, and record data quality," *Journal of Geophysical Research (Atmospheres)*, vol. 118, no. D17, p. 12734, Nov. 2013.

[3] L. L. Strow, H. Motteler, D. Tobin, H. Revercomb, S. Hannon, H. Buijs, J. Predina, L. Suwinski, and R. Glumb, "Spectral calibration and validation of the Cross-track Infrared Sounder on the Suomi NPP satellite," *Journal of Geophysical Research (Atmospheres)*, vol. 118, no. D17, p. 12486, Nov. 2013.

[4] F. Hilton, R. Armante, T. August, C. Barnet, A. Bouchard, C. Camy-Peyret, V. Capelle, L. Clarisse, C. Clerbaux, P.-F. Coheur, A. Collard, C. Crevoisier, G. Dufour, D. Edwards, F. Faijan, N. Fourrié, A. Gambacorta, M. Goldberg, V. Guidard, D. Hurtmans, S. Illingworth, N. Jacquinet-Husson, T. Kerzenmacher, D. Klaes, L. Lavanant, G. Masiello, M. Matricardi, A. McNally, S. Newman, E. Pavelin, S. Payan, E. Péquignot, S. Peyridieu, T. Phulpin, J. Remedios, P. Schlüssel, C. Serio, L. Strow, C. Stubenrauch, J. Taylor, D. Tobin, W. Wolf, and D. Zhou, "Hyperspectral Earth Observation from IASI: Five Years of Accomplishments," *Bulletin of the American Meteorological Society*, vol. 93, pp. 347–370, Mar. 2012.

[5] H. E. Motteler and L. L. Strow, "Deconvolution and translation between high spectral resolution IR sounders," https://github.com/strow/airs_deconv/blob/master/doc/decon_atbd.pdf, 2016.

[6] Wikipedia contributors, "Gaussian function," https://en.wikipedia.org/wiki/Gaussian_function, accessed 12 Nov 2017.

[7] E. M. Manning, H. H. Aumann, D. A. Elliott, and L. L. Strow, "AIRS Level 1C Algorithm Theoretical Basis," Jet Propulsion Laboratory, Version 3.0, Jan. 2015. [Online]. Available: http://eospso.gsfc.nasa.gov/sites/default/files/atbd/V6.1.0_201_AIRS_L1C_ATBD.pdf

[8] L. L. Strow, H. E. Motteler, R. G. Benson, S. E. Hannon, and S. D. Souza-Machado, "Fast computation of monochromatic infrared atmospheric transmittances using compressed look-up tables," *Journal of Quantitative Spectroscopy and Radiative Transfer*, vol. 59, no. 3 - 5, pp. 481 – 493, 1998, atmospheric Spectroscopy Applications 96. [Online]. Available: http://www.sciencedirect.com/science/article/pii/S0022407397001696

[9] Wikipedia contributors, "Moore–Penrose inverse," https://en.wikipedia.org/wiki/Moore-Penrose_inverse, accessed 12 Nov 2017.

[10] G. Strang, *Linear Algebra and Its Applications*, 2nd ed. Academic Press, 1980.

[11] Wikipedia contributors, "Norm (mathematics)," https://en.wikipedia.org/wiki/Norm_(mathematics), accessed 16 May 2018.

[12] L. Strow, S. Hannon, S. De Souza-Machado, H. Motteler, and D. Tobin, "An overview of the airs radiative transfer model," *Geoscience and Remote Sensing, IEEE Transactions on*, vol. 41, no. 2, pp. 303–313, Feb 2003.

[13] L. L. Strow, S. E. Hannon, S. De-Souza Machado, H. E. Motteler, and D. C. Tobin, "Validation of the atmospheric infrared sounder radiative transfer algorithm," *Journal of Geophysical Research: Atmospheres*, vol. 111, no. D9, 2006, d09S06. [Online]. Available: http://dx.doi.org/10.1029/2005JD006146

[14] H. E. Motteler and L. L. Strow, "Interferometric Interpolation," https://github.com/strow/airs_deconv/blob/master/doc/finterp.pdf, 2014.

[15] C. D. Barnet, J. M. Blaisdell, and J. Susskind, “Practical methods for rapid and accurate computation of interferometric spectra for remote sensing applications,” *IEEE transactions on geoscience and remote sensing*, vol. 38, no. 1, pp. 169–183, 2000.
[16] Wikipedia contributors, “Window function,” https://en.wikipedia.org/w/index.php?title=Window_function, accessed 12 Nov 2017.
[17] L. Wang, Y. Han, X. Jin, Y. Chen, and D. Tremblay, “Radiometric consistency assessment of hyperspectral infrared sounders,” *Atmospheric Measurement Techniques*, vol. 8, no. 11, p. 4831, 2015.
[18] C. Hepplewhite and L. L. Strow, “A Hyper-Spectral Multi-Sensor Infrared Radiance Data Record for Climate Trending: Validation using Simultaneous Nadir Observations,” https://github.com/clhepp/sno_paper_2016/blob/master/SNO_paper_2016.pdf, UMBC/JCET, In preparation, 2017.
[19] H. E. Motteler and L. L. Strow, “AIRS and CrIS sampling comparisons,” https://github.com/motteler/cris_telecon/blob/master/airs_cris_obs/airs_cris.pdf, 2017.

Howard E. Motteler (M ’87) received the Ph.D. degree in computer science from the University of Maryland at College Park in 1987. From 1987 to 1994 he was an Assistant Professor and from 1994 to 1998 an Associate Professor of computer science at the University of Maryland Baltimore County, and from 1992 to 1993 an NRC Research Associate at NASA/GSFC. Since 1998 (with a break from 2008 to 2011) he has been a Research Associate Professor at the Joint Center for Earth Systems Technology, Baltimore MD. His research interests include infrared sounder modeling and calibration and analysis of AIRS and CrIS data for validation and trending.

L. Larrabee Strow received the Ph.D. degree in physics from the University of Maryland, College Park, in 1981. He is currently a Research Professor with the Department of Physics, University of Maryland Baltimore County, Baltimore, MD. His work focuses on remote sensing of the Earth in the infrared using high spectral resolution satellite instruments. His primary goal is to measure climate trends using infrared sensors flown by NASA, NOAA, and EUMETSAT. To that end, he is a Science Team Member of NASAs Aqua Atmospheric InfraRed Sounder (AIRS) instrument, the NPOESS/JPSS(NOAA-20) Cross-track Infrared Sounder (CrIS) and EUMETSAT’s Infrared Atmospheric Sounding Interferometer (IASI). He also provides NASA and NOAA with the radiative transfer algorithms for the retrieval of geophysical variable using AIRS, IASI, and CrIS.